mater.scichina.com link.springer.com

Published online 28 August 2024 | https://doi.org/10.1007/s40843-024-3068-5
Sci China Mater 2024, 67(10): 3215–3224

Design principle of single-atom catalysts for sulfur reduction reaction—interplay between coordination patterns and transition metals

Wentao Zhang[1,2†], Gaoshang Zhang[1,2†], Zhaotian Xie[1,2], Xinming Zhang[1,2], Jiabin Ma[1,2], Ziyao Gao[1,2], Kuang Yu[1*] and Lele Peng[1*]

ABSTRACT **The polysulfide shuttling effect is the primary bottleneck restricting the industrial application of Li-S batteries, and the electrocatalytic sulfur reduction reaction (SRR) has emerged as an effective solution. Carbon-based single-atom catalysts (SACs), which promotes SRR, show great potential in inhibiting the shuttling effect of polysulfides. Meanwhile, the optimization and rational design of such catalysts requires a deep understanding to the fundamental SRR mechanism and remains highly nontrivial. In this work, we construct a comprehensive database of carbon-based SACs, covering different coordination patterns, heteroatoms, and transition metals. The SRR activities are determined using density functional theory calculations, revealing a synergistic effect between the p orbital of the heteroatom and the d orbital of the transition metal. This interplay underscores the critical importance of the coordination environment for SRR under the ortho-P_2C_2 structure. Regardless of the transition metal type, the ortho-P_2C_2 coordination pattern significantly enhances the SRR performance of SACs, surpassing the widely reported N_3C_1 and N_4 coordinated graphene-based SACs. Furthermore, heteroatoms with ortho-P_2C_2 may exhibit SRR activity. In a word, by using this comprehensive dataset and data-driven framework, we propose a promising novel class of coordination structure (ortho-P_2C_2 structure) and neglected design principle.**

Keywords: single-atom catalysts, ortho-P doped structure, *ab-initio* calculations, machine learning, sulfur reduction reaction

INTRODUCTION

Lithium-sulfur batteries (Li-S batteries) are considered as one of the most promising candidates for the next generation of rechargeable batteries, as they feature higher theoretical capacity and energy density than the widely used lithium-ion batteries [1–5]. The theoretical weight capacity of Li-S batteries is up to 1675 mAh g^{-1} [6], and during discharge, the maximum energy density even reaches 2600 Wh kg^{-1} [7]. Experimentally, the full packaged Li-S batteries reach a specific energy of 400–600 Wh kg^{-1}, three times that of commercial lithium-ion batteries [8]. Therefore, Li-S batteries warrant promising applications in portable electronic equipment, electric vehicles, medical equipment, and aerospace, where energy density and capacity are a key factor [9]. The high energy density of Li-S batteries is a result of the complex 16-electron conversion process, in which the S_8 ring molecules are first converted into a series of soluble lithium polysulfides and eventually into insoluble Li_2S_2/Li_2S products [10–12]. However, the shuttling effect of polysulfides and slow sulfur reduction reaction (SRR) kinetics limit the performance of Li-S batteries [13]. In order to address the problems brought by the shuttling effect in Li-S batteries, two strategies have been proposed (Scheme 1a). The first strategy is the passive strategy based on physical confinement and chemical adsorption [14–16]. While this approach can suppress polysulfide shuttling to some extent, it cannot fundamentally shut down the shuttling pathway. In contrast, the active strategy of electrocatalytic conversion of polysulfides [17–19] promotes the SRR kinetics and reduces the accumulation of polysulfide intermediates, eventually avoiding its shuttling. Naturally, the key to such electrocatalysis strategy lies in the development of high-performance electrocatalysts.

Single-atom catalysts (SACs) achieve maximal atom utilization by exposing all individual metal atoms as active centers, featuring superior catalytic activity that compensates for the high cost and resource scarcity of precious metals [20–25]. Therefore, SACs are considered to be excellent candidates for cathode electrocatalysts for SRR, specially with graphene as the substrate [26]. Currently, nitrogen (N) doping is the most common strategy to construct graphene-based SACs [27–29]. For example, Wu's group [30] used superlayered cobalt embedded in N-doped porous carbon nanosheets (Co/N-PCNSs) as a stable host for elemental sulfur and metallic lithium, improving electrocatalytic sulfur reduction performance. Lin's group [31] designed an N-doped carbon/graphene (NC/G) sheet as a sulfur host, which promotes the redox reaction kinetics of sulfur cathode thanks to abundant N active sites and high electrical conductivity. However, the N-doping strategy is still unable to meet the requirements of industrial applications [32].

Given that the electronegativity of C atom (2.55) is higher than that of P atom (2.19) but lower than N (3.04), the polarity of C–P bond is opposite to C–N bond [33,34]. Thus, when P is doped in carbon, the charged sites of P^+ are created. Unlike the N-doped graphene-based SACs, where the N atoms remain inactive, the positively charged P atoms in the P-doped graphene-based SACs are potentially active. Furthermore, P possesses a larger atomic radius than C (110 pm vs. 77 pm),

[1] Tsinghua Shenzhen International Graduate School, Tsinghua University, Shenzhen 518055, China
[2] School of Materials Science and Engineering, Tsinghua University, Beijing 100084, China
† Equally contributed to this work.
* Corresponding author (email: yu.kuang@sz.tsinghua.edu.cn; penglele@sz.tsinghua.edu.cn)

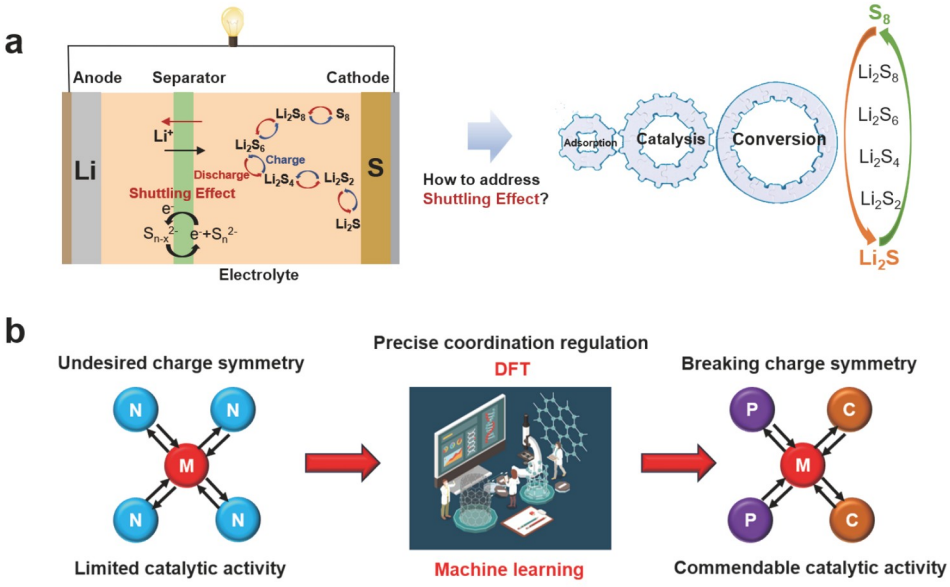

Scheme 1 Data-driven framework to address shuttling effect. (a) How to address the shuttling effect for high specific energy Li-S batteries. (b) The proposal of a new class of electrocatalyst with Ortho-P_2C_2 coordination mode via DFT and ML.

favoring the sp3-orbital configuration, which can produce high distortion in the graphene skeleton and abundant edge sites [35–37]. For S doping, the electronegativity of S (2.58) is very close to that of C (2.55), making it unlikely to significantly cause charge-neutral break of carbon. However, the high spin density induced by doping S in carbon is conducive to enhancing the electrocatalytic activity. In addition, strain-induced charge localization and lone pairs in S atoms are also favorable for chemisorption [38–40]. Therefore, it is expected that P or S doping strategy may open up new avenues for the development efficient electrocatalytic SRR [35,38,40]. Furthermore, the model used to study the catalytic activity of SACs is usually the N_4 coordination structure [41–46]. This has long led to the consideration of transition metal types as the most important factor affecting the catalytic activity of SACs, while the role played by the coordination environment has been seriously overlooked. It is well known that the N_4 coordination structure struggles to meet the performance requirements of practical industrial applications due to its high charge symmetry [47,48]. Therefore, clarifying the role of the coordination environment in the catalytic activity of SACs and discovering new coordination structures with desired performance is highly attractive to compensate for the shortcomings of classical N_4 coordination structures. It can be foreseen that there are numerous combinations of coordination patterns, type of heteroatoms, and type of transition metals, which makes it still a great challenge to clarify the interplay between coordination environment and transition metal, so as to rationally design P/S-doped SACs. It is almost impossible to explore the design space exhaustively using traditional "trial and error" methods [49]. In recent years, the rapid development of theoretical and computational tools has enabled us to understand the electronic structure of SACs in great detail, aiding the rational design of new catalysts. Meanwhile, newly emerged data-driven techniques, such as machine learning (ML) [50,51], can help us to establish the structure-activity relationship, allowing us to screen a vast number of candidates efficiently.

In this paper, we use density functional theory (DFT) calculations to establish a comprehensive dataset of graphene-based SACs with different coordination patterns, heteroatom doping, and transition metals. Facilitated with ML tools, we explore the database to understand the interplay between the coordination environments and the transition metals. A significant synergistic effect between p-orbital of heteroatoms in the substrate and the d-orbital of transition metal is found, leading to the identification of several new SAC materials with superior performance. In particular, we propose a novel coordination pattern, the ortho-P_2C_2 doped structure, which can enhance the SRR activity for 3d, 4d and 5d transition metals (Scheme 1b). The resulting activity is far superior to the widely reported N_3C_1 and N_4 coordinated graphene-based SACs. The ortho-P_2C_2 doped structure features a considerably low overpotential down to 0.042 V and a reduced Li_2S decomposition energy barrier, both of which warrant accelerated consumption of polysulfides. The stability of the newly proposed ortho-P_2C_2 SACs is also demonstrated by the cohesion energy, formation energy and molecular dynamics (MD) simulation, assuring their practical applicability.

RESULTS AND DISCUSSION

Electrocatalytic sulfur reduction activity of SACs

Thanks to the 16 electron reduction process of S_8 molecules, Li-S batteries possess an extremely high theoretical specific capacity (1675 mAh g^{-1}) and energy density (2600 Wh kg^{-1}) [6,7]. The capacity of the sulfur cathode electrode is closely related to the complex "solid-liquid-solid" multi-step reaction kinetics, especially the deposition/dissociation process of Li_2S, which contributes 3/4 of the charge-discharge capacity of the cathode. To investigate this reaction, we built several models with P/S doping atoms and 3d, 4d and 5d transition metals, corresponding to six coordination patterns (Fig. 1a, b). When the coordination number is 2, there are two coordination patterns involved: para

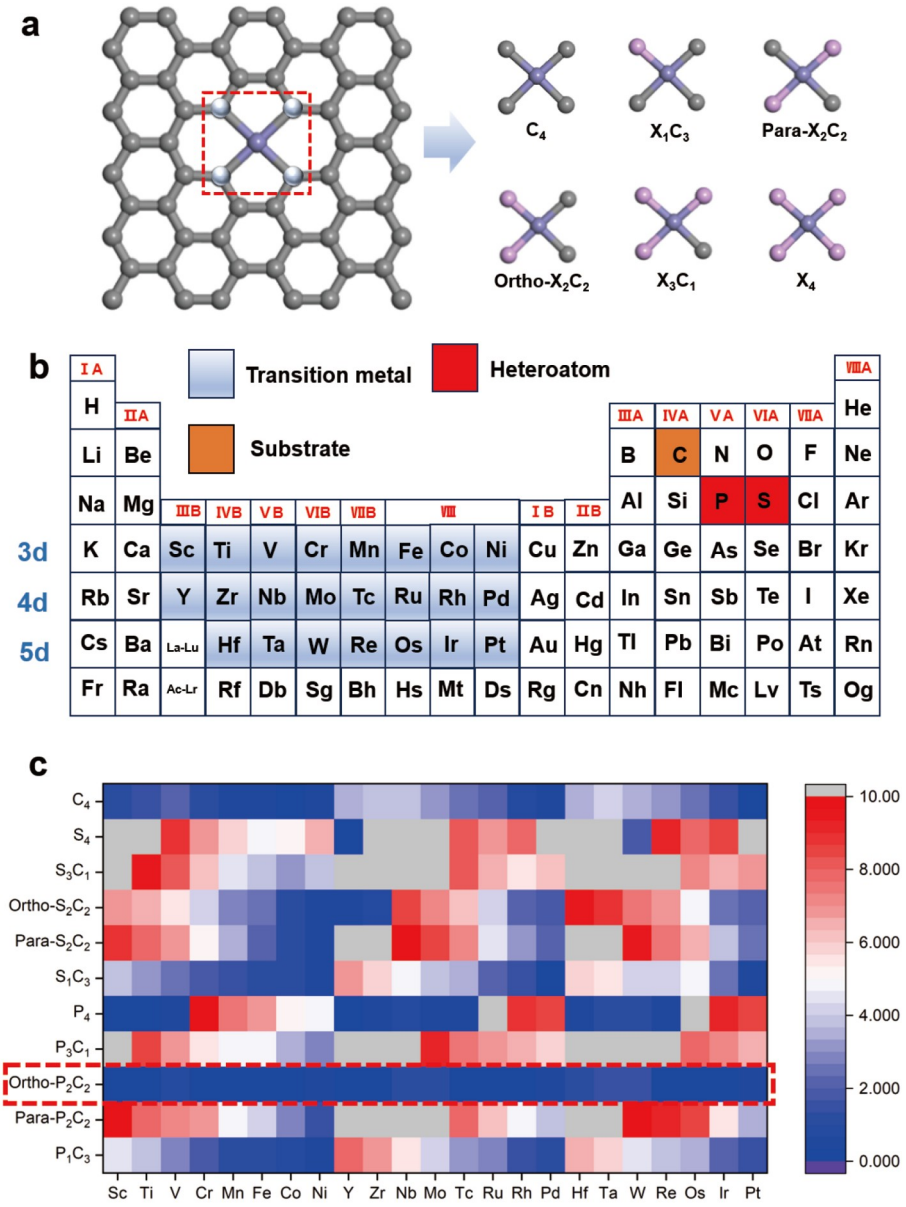

Figure 1 The computational model and electrocatalytic sulfur reduction activity of SACs. (a) The coordination patterns covered in the computational model, where X corresponds to P/S heteroatom. (b) The type of 3d (Sc, Ti, V, Cr, Mn, Fe, Co, Ni), 4d (Y, Zr, Nb, Mo, Tc, Ru, Rh, Pd) and 5d (Hf, Ta, W, Re, Os, Ir, Pt) transition metals, heteroatom (P, S) and substrate (C) involved in the computational model. (c) Overpotential of SACs covering 3d, 4d and 5d transition metals.

and ortho coordination, leading to 253 different structures in total. It should be pointed out that based on the following reasons, we only considered single doping of P or S and did not consider co doping of P and S: (1) The widely reported coordination structures are mainly single element doped structures [52–54], so setting the calculation model as P or S element single doping is more in line with the real situation; (2) the dataset composed of single doped SACs with P or S and co-doped SACs with P and S may have significant differences, which is not conducive to obtaining excellent performance of ML models. In other words, heterogeneous datasets may result in the inability to capture potential correlations between electronic properties and catalytic activity [55–59].

Considering the effect of morphology, specific surface area and hydrophilicity on catalytic activity in DFT calculation is indeed a difficult problem with low availability of calculation methods and huge calculation amount. In general, morphology, specific surface area, and hydrophilicity affect the reaction rate mainly through mesoscopic mass transport, so the above factors are often taken into account by multi-scale models coupling diffusion to electrochemical surface dynamics [60]. For the calculation model in this paper, when graphene-based SACs are used for electrocatalytic SRR, the speed determination step of intrinsic activity is the most critical factor in theory, and the influence of external factors such as morphology, specific surface area and hydrophilicity is unlikely to be the dominant factor. This is because for graphene-based SACs, most of the atoms are still carbon atoms, and the transition metal only accounts for a small part, which means that the morphology, specific surface area and hydrophilicity of graphene-based SACs with different

transition metals may be similar. Therefore, only the intrinsic activity and its corresponding velocity steps are considered in the calculation of this paper.

Targeting the decisive step ($Li_2S_2 + 2Li^+ + 2e^- \rightarrow 2Li_2S$), the overpotentials of all model graphene-based SACs were calculated (Fig. 1c). Compared with S doping, P doping exhibits lower overpotentials (Fig. 1 and Fig. S1) in average, which means that P doping is a more effective strategy to improve SRR activity. Furthermore, for P doping, different coordination modes show diametrically opposite electrocatalytic performance. The graphene-based SACs with the coordination pattern of P_3C_1 and para-P_2C_2 possess higher overpotential regardless of the transition metal type. In contrast, the ortho-P_2C_2 coordinated SACs all exhibit commendable electrocatalytic sulfur reduction activity for all transition metals (Fig. S2a). In the 20 graphene-based SACs with top performance, the ortho-P_2C_2 coordination pattern accounts for 3/5, and 5 out of the 6 graphene-based SACs with top performance feature ortho-P_2C_2 coordination pattern (Fig. 1b). This suggests that the ortho-P_2C_2 coordination pattern possesses a significant advantage over the other five coordination patterns. As for different metals, for P/S doped graphene-based SACs, there is a difference in the overpotential of 3d, 4d and 5d transition metals. The overpotentials of the 3d transition metals are the lowest, followed by the 4d and the 5d transition metals (Fig. S3).

For 3d transition metals, the overpotentials corresponding to Cr, Mn, Fe, Co and Ni are generally lower. For 4d transition metals, Ru, Rh and Pd are the better performers, while Ir and Pt are the best candidates in 5d transition metals. Through DFT calculations, six P-doped graphene-based SACs with the most excellent sulfur catalytic activity are identified, among which the overpotential of ortho-FeP_2C_2 is as low as 0.042 V (Table S1). The N doping is the most widely reported doping strategy, graphene-based SACs with N_3C_1 and N_4 coordination have been synthesized experimentally. However, in here, we found all the N_3C_1 coordination and N_4 coordination structures feature overpotentials much larger than that of ortho-FeP_2C_2 (Fig. S4). Therefore, according to our calculation, the electrocatalytic sulfur reduction activity of ortho-FeP_2C_2 is superior to all graphene-based SACs with N_3C_1 coordination and N_4 coordination. Considering the significant price advantage of Fe, the ortho-FeP_2C_2 system is proposed to be the most promising candidate for a cheap catalyst for SRR reactions in Li-S batteries, yet with a performance potentially better than all N_3C_1 and N_4 coordinated materials.

Stability and electrical properties of ortho-P doped structure

Stability evaluation of SACs with ortho-P doped structure

High stability is a prerequisite for the application of cathode catalytic materials [61], which is evaluated in this work using cohesion energy, formation energy and MD simulations. The thermodynamic stability of the material is represented by both cohesion energy and formation energy, which use isolated atoms and the most stable element as references. All the data are presented in Fig. S5. The cohesion energy of ortho-P_2C_2 and P_4 doped graphene are 7.66 eV/atom and 7.49 eV/atom, respectively (Fig. S5). The cohesion energies of graphene-based SACs are (from lower to higher): YP_4 (7.48 eV/atom), ortho-MnP_2C_2 (7.61 eV/atom), ortho-YP_2C_2 (7.62 eV/atom), ortho-FeP_2C_2 (7.63 eV/atom), ortho-ScP_2C_2 (7.63 eV/atom), and ortho-IrP_2C_2 (7.67 eV/atom), which are all more stable than carbon phosphide (4.12–6.45 eV/atom) [62] and silene (3.71 eV/atom) [63], indicating its high stability. The high stability of ortho-P doped graphene-based SACs and its precursors are also confirmed by the calculated formation energies (Fig. S5). For dynamic stability, MD simulation reveals that the kinetic energy of all the structures of the proposed ortho-P SACs with commendable electrocatalytic SRR activity and their precursors fluctuates within an extremely small range during 5 ps of simulation under 300 K, indicating no significant change in structure, i.e., high thermal stability (Figs S6 and S7). All above results verify the stabilities of the ortho-P_2C_2 coordination graphene-based SACs, making them promising for future synthesis.

Electrical property of SACs with ortho-P doped structure

Other than catalytic activity and stability, the electrical conductivity is also an important index for a good electrochemical catalyst. Therefore, we study the electrical conductivities of all ortho-P doped structures via investigating their band structures and density of states (DOS) (Figs S8 and S9). Similar to the experimentally reported SACs, the bandgaps of the proposed ortho-P doped structure are extremely narrow, indicating excellent electrical conductivities (Figs S8 and S9). For the proposed SACs, the 2p orbitals of C form the conduction band and valence band. The transition metal d orbitals of ortho-FeP_2C_2, ortho-MnP_2C_2, and ortho-IrP_2C_2 participate in the valence band. However, the metal d orbitals of ortho-YP_2C_2 and ortho-ScP_2C_2 are involved in forming the conduction band, which is similar to experimentally reported SACs (Figs S10 and S11). The DOS of ortho-P doped structure do not decrease after adsorption of LiS. Moreover, the S of LiS also contributes an obvious DOS, which means that the adsorption of LiS is beneficial for improving the conductivity of the cathode (Figs S12 and S13). Besides the electrical conductivity, we further performed work function analysis on all ortho-P SACs, which all show lower electron escape work than graphene (4.56 eV) [64]. It is also consistent with their high activities on the electrocatalytic process of SRR (Fig. S14 and Table S2). In summary, all electronic structure analysis confirms that the proposed ortho-P_2C_2-doped graphene-based SACs possesses excellent electrical properties and are suitable for SRR catalyst applications.

Electrocatalytic sulfur reduction mechanism of ortho-P doped structure

Explore sulfur reduction activity via ML

ML provides a powerful tool for revealing the interplay of the coordination environments and transition metals of SACs for electrocatalytic SRR, as long as the input descriptors are carefully chosen [65,66]. The descriptors mush be complete enough to give a comprehensive description to the physiochemical properties of SACs, while remain independent to each other to avoid numerical problems. The descriptors we use in this study are shown in Table 1. These descriptors can be categorized into DFT-calculated descriptors and elemental and structural descriptors. Considering the structure of graphene-based SACs, a number of descriptors related to coordination environments and transition metal types are used, including coordination modes of heteroatoms (such as *C*), p-orbital-related electronic properties of heteroatoms (such as p_{PS}), and transition metal types and the d-orbital-related electronic properties (for

Table 1 Descriptors employed in model training

DFT-calculated descriptors	
q_M	Bader charge transfer of metal atom
q_{PS}	Bader charge transfer of P or S atom
q_C	Bader charge transfer of C atom
ε_d	d band center of metal
d_{Ne}	d orbital electron number below Fermi level for metal
d_{unocc}	The number of unoccupied d states for metal from 0 to 3 eV
ε_p	p band center of metal atom
E_g	Band gap
E_f	Energy of Fermi level
p_{PS}	The number of p orbital electrons for P or S atom
p_C	The number of p orbital electrons for C atom
I_M	First ionization energy of metal atom
I	First ionization energy of SACs@graphene
E_N	Electronegativity of metal atom
E_M	Electron affinity of metal atom
E	Electron affinity of SACs@graphene
Z	Valence electron of metal atom
Elemental and structural descriptors	
r_M	Atomic radius of metal atom
$R_{M(I)}$	Metal(I) ion radius
$R_{M(II)}$	Metal(II) ion radius
C	Configuration
AN	Atomic number

example, ε_d, d_{Ne}, d_{unocc}). We compare the performances of seven ML models, including multiple linear regression (MLR), ridge regression, Lasso, support vector regression (SVR), Xtreme Gradient Boosting (XGBoost), decision tree (DT) and artificial neural network (ANN). The whole dataset is randomly partitioned into training and testing sets with a ratio of 3:1. Specific parameters employed in the training of each model are shown in Table S3. ANN exhibits excellent predictive ability for both training and testing data, with R^2 of 0.9631 and 0.9431, respectively (Fig. 2a, b). Meanwhile, XGBoost and DT strongly overfits the problem in the current available dataset, while other under fits with R^2 values ranging from 0.6354 to 1 (Figs S15 and S16). Therefore, we conclude that ANN is the most suitable model for overpotential prediction in this study.

Shapley additive explanation (SHAP) analysis elucidates the potential factors controlling the properties of catalytic materials. This SHAP results reveal the interplay between coordination environments and transition metals. As shown in Fig. 2c, the descriptors that are most important for overpotential prediction are independent of each other, as evidenced by the relatively low correlation coefficients between them. According to Fig. 2d, the most correlated five descriptors are p_{PS} (the number of p-orbital electrons of the P or S atom), C (configuration), E_f (the Fermi level), d_{Ne} (d orbital electron number below Fermi level for metal), and d_{unocc} (the number of unoccupied d states for metal from 0 to 3 eV). The strong correlation between coordination mode descriptors and overpotential explains the underlying mechanism behind the optimization of electrocatalytic sulfur reduction activity by ortho-P doped structure. p_{PS} and configuration highlight the regulation of the electronic properties of transition metal by graphene substrate, which may be beneficial for understanding the interplay between the active sites of transition metal and graphene substrate. Through SHAP analysis, it is found that the downward shift of p-band center of P atoms corresponds to the decrease of overpotentials, which is consistent with the results of DFT analysis. Generally, a low p-band center corresponds to stronger electron drawing effect [67], and the 3p orbital energy of P might be similar to the d orbital energy of the transition metal, thereby accepting electrons from the d-orbitals of transition metal and optimizing the hybridization degree of the d-orbitals of transition metal and the p-orbitals of S atom. It should be pointed out that for SACs, the catalytic active site is transition metal. The coordination environment generally affects catalytic performance by changing the electronic properties of transition metals. Therefore, the recognition of the coordination pattern as the most important descriptor does not mean that the catalytic active site is P or S atom, but rather because the electronic properties of the transition metal that are truly affected by the coordination environment are not recognized, resulting in not being selected as the descriptor for the training model. This also suggests an interplay between the coordination environment and the transition metal. E_f, d_{Ne} and d_{unocc} are closely related to the d-orbital electron of transition metal, which emphasizes the key role of transition metal types in the electrocatalytic sulfur reduction activity of graphene-based SACs. Through SHAP analysis, it is found that the higher the value of d_{unocc}, the lower the corresponding overpotential. This is because the more unoccupied electron energy levels in the d orbitals, the more likely optimized hybridization between the d-orbitals of transition metal and p-orbitals of S atom to occur, resulting in moderate adsorption strength that is beneficial for electrocatalytic SRR. In summary, SHAP analysis indicates the interplay between coordination environments and transition metals of graphene-based SACs together control electrocatalytic SRR, due to the synergistic effect of p-orbital electrons of heteroatoms in the substrate and d-orbital electrons of transition metal.

To further understand the interplay between the transition metal and the coordination environment, detailed DFT calculations were performed. Through structural optimization it can be found that for ortho-P doped structure, the S of the intermediate species LiS bonds not only to the transition metal, but also to one of the P atoms (Fig. S17). And the other P bonds to the transition metal. But this phenomenon is not been seen in other structures. By bader charge calculation, it is found that for ortho-P doped structure, P atom which is bonded to S is always in a state of electron loss (Fig. 3). Given that P is less electronegative than S (2.19 vs. 2.58), it is believed that the lost electrons of the P atom are transferred to the S atom. Through differential charge density calculation, we also find that both P atoms in the ortho-P structure can undertake the electrons of the transition metal, which avoids the strong adsorption between the transition metal and the intermediate species LiS (Fig. S18). The volcanic relationship between adsorption energy and overpotential also indicates that the excellent electrocatalytic SRR performance of ortho-P doped structures is due to the moderate adsorption strength of LiS intermediate specie (Fig. 3a). To

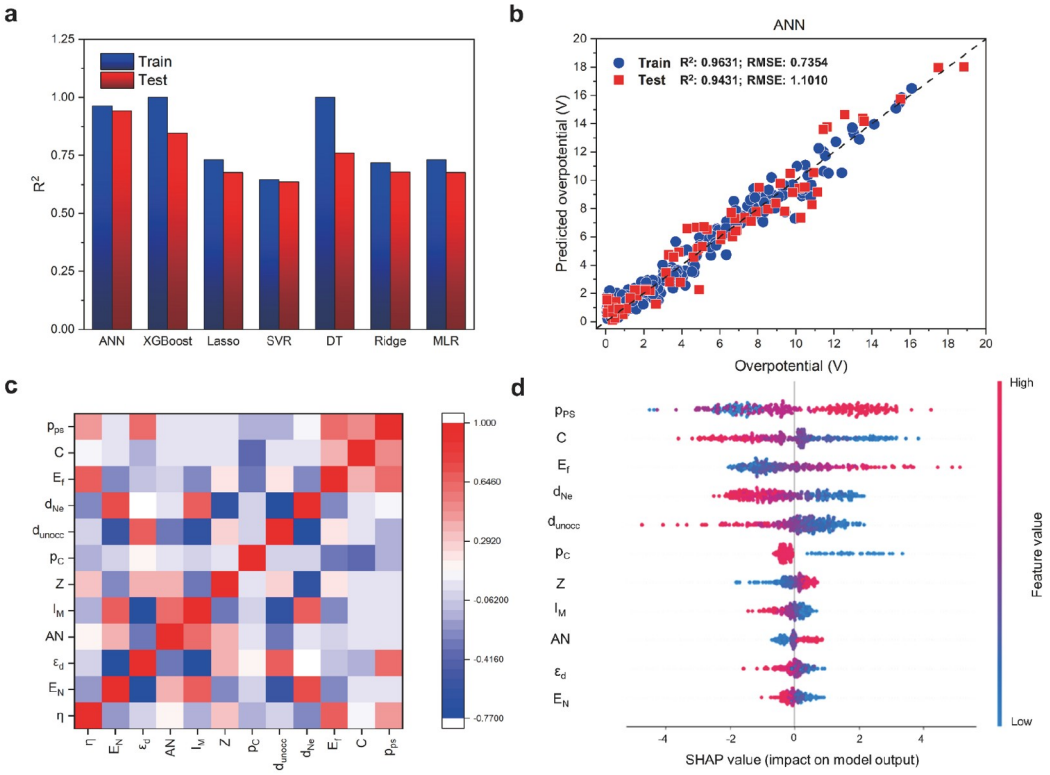

Figure 2 Exploring electrocatalytic SRR via ML. (a) R^2 of employed ML models. (b) Prediction performance of ANN. (c) The correlation between selected descriptors. (d) SHAP analysis of the ANN.

prove our conjecture, we also calculated the SRR activity of doped substrates without anchored transition metals. It is found that the unanchored ortho-P exhibits the highest overpotential, reaching 1.3525 V compared to the other five doped substrates. Therefore, ortho-P without anchored transition metals cannot be used alone for SRR and must interact with transition metals to achieve enviable SRR performance. Combining SHAP analysis and DFT calculations, we believe that the ortho-P doped structure can not only accept electrons from transition metals to avoid strong adsorption (Fig. 3b). Moreover, P, which forms a bond with S, can also serve as a bridge to transfer the extracted electrons to S, thus exhibiting commendable SRR activity. It should be emphasized that previously reported work has demonstrated that the coordination environment of SACs can significantly affect the electronic properties of transition metals, thus playing a crucial role in SRR activity. For example, W/NG with a unique W–O_2N_2–C coordination structure exhibits high adsorption capacity and SRR catalytic activity, due to the special effect of W–O coordination configuration on regulating the electronic structure and adsorption behavior of active sites [68]. Thanks to the fully accessible Fe-N/C active sites implanted within dual N and P-doped carbon framework, the catalytic activity of FeN_6 NPC with customized coordination structure towards lithium polysulfides has been significantly enhanced [69]. By introducing S atoms to replace N atoms in the first coordination shell, the electron distribution of Co sites can be adjusted to enhance their anchoring ability to lithium polysulfides, resulting in higher surface capacity and cycling stability of batteries using S@S-Co-SACs/NSC cathode [70]. In a word, these results validate the design principles presented here.

Considering that transition metals dispersed on the substrate are generally the real catalytic sites of SACs, the catalytic activity of heteroatoms is lower than that of transition metals. And, ortho-P doped structure generally exhibits surprising electrocatalytic SRR activity across all the transition metals involved. Therefore, this interplay can be extended to a specific coordination pattern (ortho-P) which is decisive for electrocatalytic SRR in some cases. On the one hand, the specific coordination pattern (ortho-P) can significantly modulate the electronic properties of transition metals. On the other hand, heteroatoms configured with the ortho-P pattern may exhibit certain electrocatalytic SRR activity, such as partial positively charged P atoms with ortho-coordination can serve as active sites [33,34].

Electrocatalytic conversion of polysulfides

In this section we analyze the details of the electronic structure of the ortho-FeP_2C_2 catalyst along the SRR reaction pathway. As shown in Fig. S19, the adsorption strength of ortho-FeP_2C_2 for all sulfur species (S_8, Li_2S_8, Li_2S_6, Li_2S_4, Li_2S_2, and Li_2S) is moderate, which facilitates the full reduction of S. The differential charge density indicates that there is significant charge transfer between ortho-FeP_2C_2 and all polysulfides (Fig. S20). The electrons are primarily transferred from the S atoms to the vicinity of the Fe atom, so the central Fe indeed facilitates the reduction of S species. The DOS of ortho-FeP_2C_2 adsorbing lithium-sulfur clusters is shown in Figs S21 and S22. The DOS of ortho-FeP_2C_2 is significantly enhanced after polysulfide adsorption, thanks to the S of lithium-sulfur clusters. This indicates that the adsorption of polysulfides can improve the electrical conductivity of the system. The low band gaps indicate the metal-like conductivity

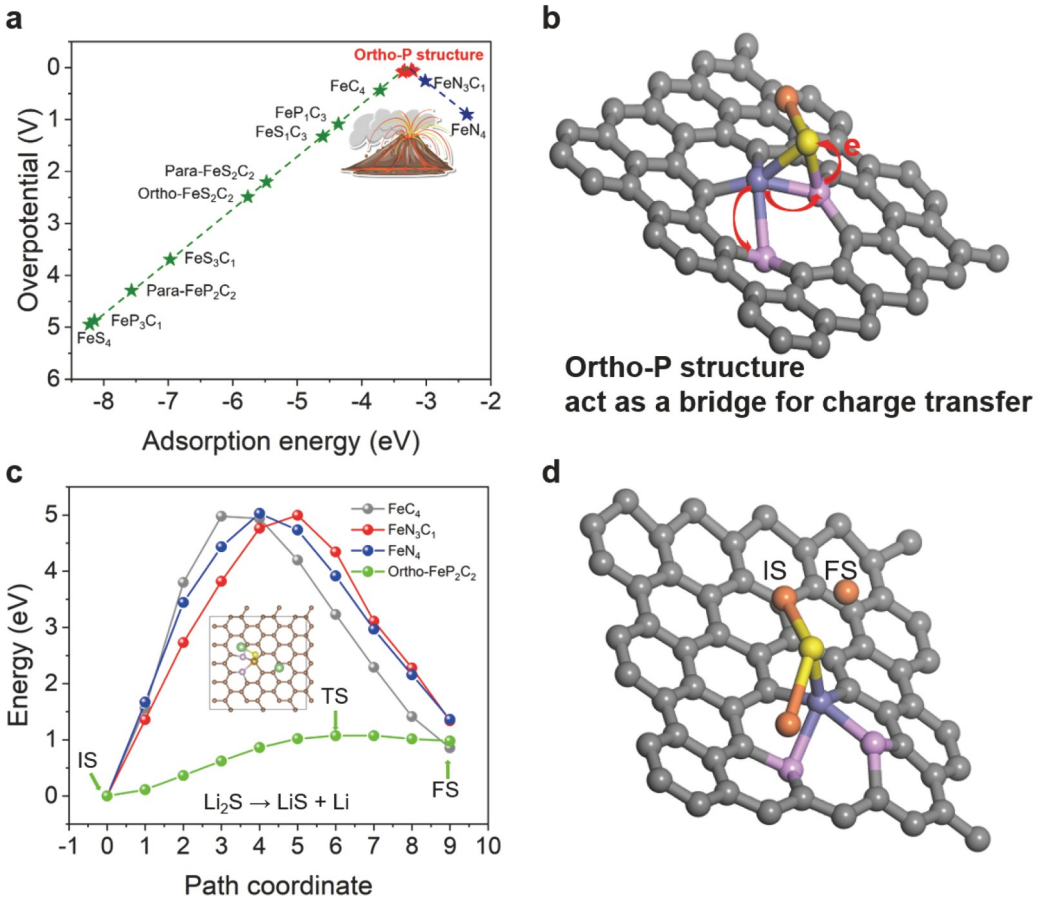

Figure 3 Electrocatalytic SRR mechanism and Li_2S decomposition of ortho-P doped structure. (a) The volcanic relationship between adsorption energy and overpotential. (b) The catalytic mechanism of ortho-P doped structure for SRR. (c) Li_2S decomposition energy barrier. (d) Li_2S decomposition pathway. The colors of the C, P, Fe, Li, and S atoms correspond to gray, lavender, brownish blue, dark orange, and yellow, respectively. IS: initial state, TS: transition state, FS: final state.

of ortho-FeP_2C_2 with adsorbing lithium-sulfur clusters. For Li_2S, Li_2S_4, Li_2S_6, and Li_2S_8, the DOS at the conduction band edge significantly increases. In addition, ortho-FeP_2C_2 obtained electrons from lithium-sulfur clusters, which helps to enhance the conductivity of ortho-FeP_2C_2. Therefore, the low bandgap and increased DOS enhances the conductivity of the cathode of Li-S batteries, thereby improving the battery rate performance.

It should be noted that the decomposition of the final discharge product Li_2S is a key factor affecting the charge-discharge performance of Li-S batteries [71]. Therefore, the decomposition energy barrier and pathway of the final discharge product Li_2S on ortho-FeP_2C_2 surface was calculated. The dissociation process includes the decomposition of Li_2S into individual Li^+ and LiS ($Li_2S \rightarrow LiS + Li^+ + e^-$) [72]. The dissociation energy barrier and dissociation pathway of Li_2S on the surface of ortho-FeP_2C_2 are shown in Fig. 3c, d. The decomposition energy barrier of Li_2S on the surface of ortho-FeP_2C_2 is 1.07 eV, much lower than the commonly studied FeC_4 (4.97 eV), FeN_3C_1 (4.99 eV) and FeN_4 (5.03 eV). The low decomposition energy barrier of Li_2S indicates that the ortho-P doped structure can improve the charge and discharge kinetics of Li-S batteries.

CONCLUSIONS

In conclusion, we explore a comprehensive dataset of graphene-based SACs covering different coordination patterns, heteroatoms and transition metals in detail through *ab-initio* calculation and ML. The interplay between the coordination environment and the transition metal is revealed, which is attributed to the synergistic effect between the p-orbital of the heteroatoms in the substrate and the d-orbital of the transition metal. This interplay can be extended to the fact that the coordination environment plays a decisive role in electrocatalytic SRR. Accordingly, a novel coordination structure (ortho-P_2C_2 structure) is proposed, which exhibits great advantages of electrocatalytic SRR for 3d, 4d and 5d transition metals. The resulting advantages including a considerably low overpotential down to 0.042 V and a reduced Li_2S decomposition energy barrier, which is far superior to that of the experimentally N_3C_1 and N_4 coordinated SACs. Moreover, the proposed ortho-P doped structure exhibits excellent stability, which assures its practical applicability. In this work, the interplay between coordination environments and transition metals for electrocatalytic SRR is elucidated through a data-driven framework, thus illuminating a novel class of SAC materials with specific structure and commendable catalytic properties. It should also be noted that P and S co-doping has not been discussed in this study, considering that such doping may lead to new discoveries similar to ortho-P_2C_2 coordination structure.

Received 26 June 2024; accepted 30 July 2024; published online 28 August 2024

1 Guo Z, Song X, Wang X, *et al.* Inhibition of polysulfide shuttling in high-polarity electrolytes via liquid/quasi-solid interface in lithium-sulfur batteries. Sci China Mater, 2023, 66: 505–512
2 Zhang Z, Wu DH, Zhou Z, *et al.* Sulfur/nickel ferrite composite as cathode with high-volumetric-capacity for lithium-sulfur battery. Sci China Mater, 2019, 62: 74–86
3 Cheng Q, Xu W, Qin S, *et al.* Full dissolution of the whole lithium sulfide family (Li_2S_8 to Li_2S) in a safe eutectic solvent for rechargeable lithium–sulfur batteries. Angew Chem Int Ed, 2019, 58: 5557–5561
4 Ma F, Chen Z, Srinivas K, *et al.* VN quantum dots anchored N-doped carbon nanosheets as bifunctional interlayer for high-performance lithium-metal and lithium-sulfur batteries. Chem Eng J, 2023, 459: 141526
5 Ma F, Srinivas K, Zhang X, *et al.* Mo_2N quantum dots decorated N-doped graphene nanosheets as dual-functional interlayer for dendrite-free and shuttle-free lithium-sulfur batteries. Adv Funct Mater, 2022, 32: 2206113
6 Seh ZW, Sun Y, Zhang Q, *et al.* Designing high-energy lithium–sulfur batteries. Chem Soc Rev, 2016, 45: 5605–5634
7 Xiong P, Peng S, Zhang L, *et al.* Supramolecular interactions enable pseudo-nanophase separation for constructing an ion-transport highway. Chem, 2023, 9: 592–606
8 Tian Y, Zhao Y, Zhang Y, *et al.* Construction of oxygen-deficient La$(OH)_3$ nanorods wrapped by reduced graphene oxide for polysulfide trapping toward high-performance lithium/sulfur batteries. ACS Appl Mater Interfaces, 2019, 11: 23271–23279
9 Zhang Q, Huang Q, Hao S, *et al.* Polymers in lithium-sulfur batteries. Adv Sci, 2021, 9: 2103798
10 Liu R, Wei Z, Peng L, *et al.* Establishing reaction networks in the 16-electron sulfur reduction reaction. Nature, 2024, 626: 98–104
11 Pang Q, Liang X, Kwok CY, *et al.* Advances in lithium–sulfur batteries based on multifunctional cathodes and electrolytes. Nat Energy, 2016, 1: 16132
12 Yu B, Huang A, Srinivas K, *et al.* Outstanding catalytic effects of 1T'-$MoTe_2$ quantum dots@3D graphene in shuttle-free Li-S batteries. ACS Nano, 2021, 15: 13279–13288
13 Zhang Y, Kang C, Zhao W, *et al.* d-p hybridization-induced "trapping–coupling–conversion" enables high-efficiency Nb single-atom catalysis for Li-S batteries. J Am Chem Soc, 2023, 145: 1728–1739
14 Wang Z, Shen J, Liu J, *et al.* Self-supported and flexible sulfur cathode enabled via synergistic confinement for high-energy-density lithium-sulfur batteries. Adv Mater, 2019, 31: e1902228
15 Niu S, Zhang SW, Shi R, *et al.* Freestanding agaric-like molybdenum carbide/graphene/N-doped carbon foam as effective polysulfide anchor and catalyst for high performance lithium sulfur batteries. Energy Storage Mater, 2020, 33: 73–81
16 Jin Z, Zhao M, Lin T, *et al.* Rational design of well-dispersed ultrafine CoS_2 nanocrystals in micro–mesoporous carbon spheres with a synergistic effect for high-performance lithium–sulfur batteries. J Mater Chem A, 2020, 8: 10885–10890
17 Yang Y, Zhong Y, Shi Q, *et al.* Electrocatalysis in lithium sulfur batteries under lean electrolyte conditions. Angew Chem Int Ed, 2018, 57: 15549–15552
18 Du L, Wu Q, Yang L, *et al.* Efficient synergism of electrocatalysis and physical confinement leading to durable high-power lithium-sulfur batteries. Nano Energy, 2019, 57: 34–40
19 Peng L, Wei Z, Wan C, *et al.* A fundamental look at electrocatalytic sulfur reduction reaction. Nat Catal, 2020, 3: 762–770
20 Chen L, Sun Y, Chang Z, *et al.* Single-atomic nickel supported on nitrogen-doped porous carbon to boost polysulfide conversion in lithium-sulfur batteries. Sci China Mater, 2024, 67: 1938–1946
21 Li H, Cao C, Liu J, *et al.* Cobalt single atoms anchored on N-doped ultrathin carbon nanosheets for selective transfer hydrogenation of nitroarenes. Sci China Mater, 2019, 62: 1306–1314
22 Li X, Huang X, Xi S, *et al.* Single cobalt atoms anchored on porous N-doped graphene with dual reaction sites for efficient fenton-like catalysis. J Am Chem Soc, 2018, 140: 12469–12475
23 Chen K, Ma D, Zhang Y, *et al.* Urea electrosynthesis from nitrate and CO_2 on diatomic alloys. Adv Mater, 2024, 36: 2402160
24 Liu P, Liu Y, Wang K, *et al.* Revealing the role of electrode potential micro-environments in single Mn atoms for carbon dioxide and oxygen electrolysis. Nano Res, 2024,
25 Zhang G, Wang G, Wan Y, *et al.* Ampere-level nitrate electroreduction to ammonia over monodispersed Bi-doped FeS_2. ACS Nano, 2023, 17: 21328–21336
26 Xie S, Chen X, Wang C, *et al.* Role of the metal atom in a carbon-based single-atom electrocatalyst for Li-S redox reactions. Small, 2022, 18: e2200395
27 Fei H, Dong J, Feng Y, *et al.* General synthesis and definitive structural identification of MN_4C_4 single-atom catalysts with tunable electrocatalytic activities. Nat Catal, 2018, 1: 63–72
28 Sun M, Ji J, Hu M, *et al.* Overwhelming the performance of single atoms with atomic clusters for platinum-catalyzed hydrogen evolution. ACS Catal, 2019, 9: 8213–8223
29 Wang H, Shi F, Pu M, *et al.* Theoretical study on nitrobenzene hydrogenation by N-doped carbon-supported late transition metal single-atom catalysts. ACS Catal, 2022, 12: 11518–11529
30 Liu S, Li J, Yan X, *et al.* Superhierarchical cobalt-embedded nitrogen-doped porous carbon nanosheets as two-in-one hosts for high-performance lithium-sulfur batteries. Adv Mater, 2018, 30: 1706895
31 Xu H, Jiang Q, Zhang B, *et al.* Integrating conductivity, immobility, and catalytic ability into high-N carbon/graphene sheets as an effective sulfur host. Adv Mater, 2020, 32: 1906357
32 Yang F, Liang C, Yu H, *et al.* Phosphorus-doped graphene aerogel as self-supported electrocatalyst for CO_2-to-ethanol conversion. Adv Sci, 2022, 9: 2202006
33 Patel MA, Luo F, Khoshi MR, *et al.* P-doped porous carbon as metal free catalysts for selective aerobic oxidation with an unexpected mechanism. ACS Nano, 2016, 10: 2305–2315
34 Zheng X, Wu J, Cao X, *et al.* N-, P-, and S-doped graphene-like carbon catalysts derived from onium salts with enhanced oxygen chemisorption for Zn-air battery cathodes. Appl Catal B-Environ, 2019, 241: 442–451
35 Wu G. Current challenge and perspective of PGM-free cathode catalysts for PEM fuel cells. Front Energy, 2017, 11: 286–298
36 Zhang C, Mahmood N, Yin H, *et al.* Synthesis of phosphorus-doped graphene and its multifunctional applications for oxygen reduction reaction and lithium ion batteries. Adv Mater, 2013, 25: 4932–4937
37 Liu Z, Peng F, Wang H, *et al.* Phosphorus-doped graphite layers with high electrocatalytic activity for the O_2 reduction in an alkaline medium. Angew Chem Int Ed, 2011, 50: 3257–3261
38 Jeon IY, Choi HJ, Jung SM, *et al.* Large-scale production of edge-selectively functionalized graphene nanoplatelets via ball milling and their use as metal-free electrocatalysts for oxygen reduction reaction. J Am Chem Soc, 2013, 135: 1386–1393
39 Yang Z, Yao Z, Li G, *et al.* Sulfur-doped graphene as an efficient metal-free cathode catalyst for oxygen reduction. ACS Nano, 2012, 6: 205–211
40 Ma Z, Dou S, Shen A, *et al.* Sulfur-doped graphene derived from cycled lithium-sulfur batteries as a metal-free electrocatalyst for the oxygen reduction reaction. Angew Chem Int Ed, 2015, 54: 1888–1892
41 Xing H, Arif M, He G, *et al.* Insights into the critical roles of γN atoms in understanding the oxygen reduction on MOF-derived single-atom catalysts. Sci China Mater, 2023, 66: 3200–3212
42 Li L, Li N, Xia J, *et al.* Post-synthetic electrostatic adsorption-assisted fabrication of efficient single-atom Fe-N-C oxygen reduction catalysts for Zn-air batteries. Sci China Mater, 2023, 66: 992–1001
43 Li Y, Zhou P, Li H, *et al.* A freestanding flexible single-atom cobalt-based multifunctional interlayer toward reversible and durable lithium-sulfur batteries. Small Methods, 2020, 4: 1900701
44 Du Z, Chen X, Hu W, *et al.* Cobalt in nitrogen-doped graphene as single-atom catalyst for high-sulfur content lithium–sulfur batteries. J Am Chem Soc, 2019, 141: 3977–3985
45 Kim J, Kim S, Jung E, *et al.* Atomic structure modification of Fe–N–C catalysts via morphology engineering of graphene for enhanced con-

version kinetics of lithium–sulfur batteries. Adv Funct Mater, 2022, 32: 2110857
46 Wang J, Zhang J, Duan S, *et al.* Lithium atom surface diffusion and delocalized deposition propelled by atomic metal catalyst toward ultrahigh-capacity dendrite-free lithium anode. Nano Lett, 2022, 22: 8008–8017
47 Zhou S, Wei W, Cai X, *et al.* Customizing highly asymmetrical coordination microenvironment into *P*-block metal single-atom sites to boost electrocatalytic CO_2 reduction. Adv Funct Mater, 2023, 34: 2311422
48 Cheng XF, He JH, Ji HQ, *et al.* Coordination symmetry breaking of single-atom catalysts for robust and efficient nitrate electroreduction to ammonia. Adv Mater, 2022, 34: e2205767
49 Ding R, Chen Y, Chen P, *et al.* Machine learning-guided discovery of underlying decisive factors and new mechanisms for the design of nonprecious metal electrocatalysts. ACS Catal, 2021, 11: 9798–9808
50 Chen X, Liu X, Shen X, *et al.* Applying machine learning to rechargeable batteries: From the microscale to the macroscale. Angew Chem Int Ed, 2021, 60: 24354–24366
51 Mai H, Le TC, Chen D, *et al.* Machine learning for electrocatalyst and photocatalyst design and discovery. Chem Rev, 2022, 122: 13478–13515
52 Day O, Khoshgoftaar TM. A survey on heterogeneous transfer learning. J Big Data, 2017, 4: 29
53 Ding S, Barr JA, Lyu Z, *et al.* Effect of phosphorus modulation in iron single-atom catalysts for peroxidase mimicking. Adv Mater, 2024, 36: 2209633
54 Duan T, Wang L, Ma Z, *et al.* Theoretical insights into single-atom catalysts supported on N-doped defective graphene for fast reaction redox kinetics in lithium-sulfur batteries. Small, 2023, 19: 2303760
55 Sun Y, Cao J, Li Q, *et al.* Identifying key factors of peroxymonosulfate activation on single-atom M–N–C catalysts: A combined density functional theory and machine learning study. J Mater Chem A, 2023, 11: 16586–16594
56 Wang T, Sang X, Zheng W, *et al.* Gas diffusion strategy for inserting atomic iron sites into graphitized carbon supports for unusually high-efficient CO_2 electroreduction and high-performance Zn-CO_2 batteries. Adv Mater, 2020, 32: 2002430
57 Wu Q, Wu H, Zhou X, *et al.* Online transfer learning with multiple homogeneous or heterogeneous sources. IEEE Trans Knowl Data Eng, 2017, 29: 1494–1507
58 Yang L, Jing L, Yu J, *et al.* Learning transferred weights from co-occurrence data for heterogeneous transfer learning. IEEE Trans Neural Netw Learn Syst, 2016, 27: 2187–2200
59 Zhang Y, Ye S, Gao M, *et al.* N-doped graphene supported Cu single atoms: Highly efficient recyclable catalyst for enhanced C–N coupling reactions. ACS Nano, 2022, 16: 1142–1149
60 Heenen HH, Pillai HS, Reuter K, *et al.* Exploring mesoscopic mass transport effects on electrocatalytic selectivity. Nat Catal, 2024, 7: 847–854
61 Hu H, Wang J, Tao P, *et al.* Stability of single-atom catalysts for electrocatalysis. J Mater Chem A, 2022, 10: 5835–5849
62 Zhou S, Wang M, Wang J, *et al.* Carbon phosphides: Promising electric field controllable nanoporous materials for CO_2 capture and separation. J Mater Chem A, 2020, 8: 9970–9980
63 Hu W, Wu X, Li Z, *et al.* Porous silicene as a hydrogen purification membrane. Phys Chem Chem Phys, 2013, 15: 5753
64 Yan R, Zhang Q, Li W, *et al.* Determination of graphene work function and graphene-insulator-semiconductor band alignment by internal photoemission spectroscopy. Appl Phys Lett, 2012, 101: 022105
65 Zheng Y, Yao Y, Ou J, *et al.* A review of composite solid-state electrolytes for lithium batteries: Fundamentals, key materials and advanced structures. Chem Soc Rev, 2020, 49: 8790–8839
66 Yao N, Chen X, Fu ZH, *et al.* Applying classical, *ab initio*, and machine-learning molecular dynamics simulations to the liquid electrolyte for rechargeable batteries. Chem Rev, 2022, 122: 10970–11021
67 Zhang Q, Gao R, Li Z, *et al.* Manipulating the conversion kinetics of polysulfides by engineering oxygen p-band of halloysite for improved Li-S batteries. Small, 2022, 18: 2105661
68 Wang P, Xi B, Zhang Z, *et al.* Atomic tungsten on graphene with unique coordination enabling kinetically boosted lithium–sulfur batteries. Angew Chem Int Ed, 2021, 60: 15563–15571
69 Faheem M, Yin X, Shao R, *et al.* Efficient polysulfide conversion by Fe-N/C active sites anchored in N, P- doped carbon for high-performance lithium-sulfur batteries. J Alloys Compd, 2022, 922: 166132
70 Sun T, Huang F, Liu J, *et al.* Strengthened d-p orbital-hybridization of single atoms with sulfur species induced bidirectional catalysis for lithium-sulfur batteries. Adv Funct Mater, 2023, 33: 2306049
71 Zhou G, Tian H, Jin Y, *et al.* Catalytic oxidation of Li_2S on the surface of metal sulfides for Li-S batteries. Proc Natl Acad Sci USA, 2017, 114: 840–845
72 Chen L, Liu Y, Ashuri M, *et al.* Li_2S encapsulated by nitrogen-doped carbon for lithium sulfur batteries. J Mater Chem A, 2014, 2: 18026–18032

Acknowledgement This work was supported by the Scientific Research Start-up Funds of Tsinghua SIGS (QD2021018C to Peng L), the National Natural Science Foundation of China (20231710015 and 22209096 to Peng L), GuangDong Basic and Applied Basic Research Foundation (2023A1515010059 to Peng L), Shenzhen Fundamental Research Program (JCYJ20220530143003008 to Peng L) and Shenzhen Science and Technology Program (ZDSYS20230626091100001). The authors would like to thank Jie Li (Nanjing University) and Xinzhu Wang (Nanjing University) for providing technical support and National Supercomputing Center Guangzhou for providing computing resources.

Author contributions Zhang W carried out the DFT computations, machine learning, investigation, formal analysis, and original draft preparation. Zhang G carried out the machine learning, investigation, formal analysis, and original draft preparation. Xie Z, Zhang X, Ma J, Gao Z carried out the formal analysis and validation. Yu K and Peng L carried out the supervision, draft reviewing and editing, conceived and supervised the research, and directed the manuscript writing and revision. All the authors assisted in writing and revising the manuscript. All authors read and approved the final manuscript.

Conflict of interest The authors declare that they have no conflict of interest.

Supplementary information Supplementary materials are available in the online version of the paper.

Wentao Zhang is currently a PhD student at Tsinghua Shenzhen International Graduate School/School of Materials, Tsinghua University, under the supervision of Professors Lele Peng and Kuang Yu. His research interests are theoretical design and molecular modeling of two-dimensional materials for energy storage and conversion.

Gaoshang Zhang is currently a Master's student at Tsinghua Shenzhen International Graduate School, Tsinghua University under the supervision of Professor Kuang Yu. His research interests are mainly in machine learning force fields and molecular dynamics simulation.

Kuang Yu is an associate professor and doctoral supervisor of Tsinghua Shenzhen International Graduate School, Tsinghua University. Professor Kuang Yu's research interests focus on theoretical and computational modelling of material systems, utilizing both *ab initio* and molecular mechanics approaches.

Lele Peng is an associate professor and doctoral supervisor of Tsinghua Shenzhen International Graduate School, Tsinghua University. His research interests are mainly in rational synthesis and structural engineering of 2D energy and catalysis materials.

用于硫还原反应的单原子催化剂的设计原则—配位模式与过渡金属的相互作用

张文涛[1,2†], 张高尚[1,2†], 谢昭天[1,2], 张新明[1,2], 马家宾[1,2], 高子耀[1,2], 余旷[1*], 彭乐乐[1*]

摘要 多硫化物穿梭是制约锂硫电池产业化的主要瓶颈，电催化硫还原(SRR)被认为是一种有效解决方案. 碳基单原子催化剂(SACs)能够显著促进SRR，同时，这种催化剂的优化和理性设计需要对SRR基本机制有深入了解. 在这项工作中，构建了涵盖不同配位模式、杂原子和过渡金属类型的全面的碳基SACs数据库. 利用密度泛函理论计算了相应SACs的SRR活性，揭示了杂原子p轨道和过渡金属d轨道之间的协同效应. 这种相互作用强调了配位环境对SRR活性的极端重要性. 无论过渡金属类型如何，ortho-P_2C_2配位模式均显著提高SACs的SRR性能，使得相应的SRR性能远远超过广泛报道的N_3C_1和N_4配位SACs. 此外，具有ortho-P_2C_2结构的杂原子可能表现出SRR活性. 总之，提出了一类有前途的新型配位结构(ortho-P_2C_2)和被忽略的设计原则.